3-D Analysis of Core Material Effects of Motors on Torque and Iron Loss Characteristics

Yoshihiro Kawase*, Tadashi Yamaguchi*, Toshinori Okouchi*, Göran Nord and Koki Kanno*****

Abstract - In this paper, a surface permanent magnet motor made of the Soft Magnetic Composites (SMC) is analysed using the 3-D finite element method. By comparing with the motor made of the silicon steel sheets, the usefulness of the SMC for the eddy current loss is clarified quantitatively.

Keywords: 3-D finite element method, soft magnetic composites, silicon steel sheet, eddy current loss, hysteresis loss

1. Introduction

SOFT Magnetic Composites (SMC) are made from insulated iron powders, which are developed by Höganäs AB. The conductivity is relatively small as the particles are electrically insulated from each other [1]. Therefore, the SMC can be used in various areas of the electrical apparatus. In this paper, we calculated the iron loss of the surface permanent motor made of the SMC using the 3-D finite element method taking into account eddy currents [2], and compared the calculated results with those of the motor made of the silicon steel sheets. Consequently, the usefulness of the SMC is clarified for the iron loss quantitatively.

2. Magnetic field Analysis

2.1 Magnetic Field Analysis

The fundamental equations of the magnetic field can be written using the magnetic vector potential A and the electric scalar potential ϕ as follows:

$$\mathrm{rot}(\nu \mathrm{rot} A) = J_0 + J_e + \nu_0 \mathrm{rot} M \tag{1}$$

$$J_e = -\sigma\left(\frac{\partial A}{\partial t} + \mathrm{grad}\ \phi\right) \tag{2}$$

$$\mathrm{div}\ J_e = 0 \tag{3}$$

where ν is the reluctivity, ν_0 is the reluctivity of the vacuum, J_0 is the exciting current density, J_e is the eddy current density, M is the magnetization, and σ is the conductivity.

2.2 Calculation of Eddy Current Loss

The eddy current loss W_{ed} is given as follows:

$$W_{ed} = \frac{1}{\tau/2}\int_t^{t+\tau/2}\left\{\int_{V_e}\frac{(J_e)^2}{\sigma}dv\right\}dt \tag{4}$$

where τ is the period of the eddy current waveform, V_e is the region of the conductor.

The conductivity of laminated core of silicon steel sheet is assumed to take into no account of the eddy current in the calculation. Therefore, the eddy current loss in silicon steel sheet can not be calculated using (4). Therefore, the eddy current loss W_{ed} without skin effects is estimated as follows [3]:

$$W_{ed} = \frac{K_e D}{2\pi^2}\int_{iron}\frac{1}{N}\sum_{k=1}^{N}\left\{\left(\frac{B_r^{k+1}-B_r^{k}}{\Delta t}\right)^2 + \left(\frac{B_\theta^{k+1}-B_\theta^{k}}{\Delta t}\right)^2 + \left(\frac{B_z^{k+1}-B_z^{k}}{\Delta t}\right)^2\right\}dv \tag{5}$$

where K_e is the coefficient of the eddy current loss, D is the density of the steel sheet, N is the number of iteration of analysis step, and Δt is the time interval of the step-by-step method.

* Y. Kawase, T. Yamaguchi and T. Okouchi are with the Department of Information Science, Gifu University, 1-1, Yanagido, Gifu, 501-1193, Japan. (kawase@info.gifu-u.ac.jp)
** G. Nord is with the Magnet Development, Höganäs AB, SE-263 83, Höganäs, Sweden. (goran.nord@hoganas.com)
*** K. Kanno is with the Technical Support Department, Höganäs Japan K.K. AKASAKA SHASTA EAST, 2-19, Akasaka 4-chome, Minato-ku, Tokyo, 107-0052, Japan. (koki.kanno@hoganas.com)
Received June 7, 2005 ; Accepted August 23, 2005

2.3 Calculation of Hysteresis Loss

The hysteresis loss W_{hy} taking into account the major and minor loops of the hysteresis loop can be estimated as follows [3]:

$$W_{hy} = \frac{K_h D}{T} \sum_{i=1}^{NE} \frac{\Delta V_i}{2} \left(\sum_{j=1}^{Npr^i} \left(B_{mr}{}^{ij}\right)^2 + \sum_{j=1}^{Np\theta^i} \left(B_{m\theta}{}^{ij}\right)^2 + \sum_{j=1}^{Npz^i} \left(B_{mz}{}^{ij}\right)^2 \right) \quad (6)$$

where K_h is the coefficient of the hysteresis loss, D is the density of magnetic material, T is the period of analysis time, NE is the number of the elements in magnetic material, and ΔV_i is the volume of the i-th element. $N_{pr}{}^i$, $N_{p\theta}{}^i$ and $N_{pz}{}^i$ are the number of the maximum or minimum value of the flux density of the radial direction, the rotation direction and the z-direction of the i-th element, respectively. $B_{mr}{}^{ij}$, $B_{m\theta}{}^{ij}$ and $B_{mz}{}^{ij}$ are the amplitude of the flux density of major and minor hysteresis loops of the radial direction, the rotation direction and the z-direction, respectively.

A. Double Nodes Technique [4]

The flat elements conventionally used for the small air gap. The flat elements make the convergence of ICCG and the accuracy of the solution worse. The double nodes technique can take the electrical insulation of conductors without the mesh for the air gap into account. Fig. 1 shows the chains of nodes for ϕ around an air gap. In the conventional technique, the mesh for the air gap is prepared to isolate the conductors as shown in Fig. 1 (a). On the other hand, in the double nodes technique, two conductors adjoin each other as shown in Fig. 1 (b), and two ϕ are prepared for on one node of the boundary line between the conductors. One belongs to one conductor and the other belongs to another conductor. Using this technique the isolated eddy currents can be calculated without the mesh of the air gap.

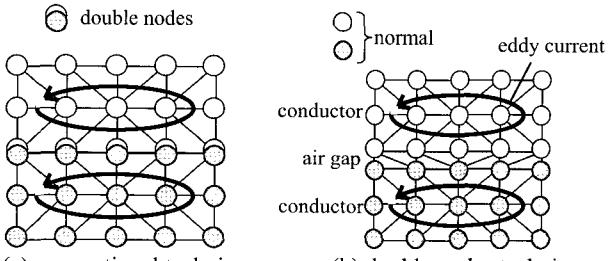

(a) conventional technique (b) double nodes technique

Fig. 1 Overview of double nodes technique

3. Analyzed Model and Condition

Fig. 2 shows the analyzed models of a surface permanent magnet motor. In this paper, three patterns of the model are analyzed. Table I shows the analysis patterns of the model. Model A is modeled by Höganäs AB, in which the rotor and the stator are made of the SMC [5]. The stator of Model A consists of several cores. The shape of core made of the SMC can be changed easily, since the SMC core is made out of insulated and compacted iron powder and not laminated sheets. Therefore, the teeth and the yoke of Model A are higher than the poles in order to distribute the flux three dimensionally in the cores. The rotor and the stator of Models B and C are made of the silicon steel sheets. The height of the rotor of Model B is higher than that of Model C, and the height of the rotor of Model B is the same as that of Model A, and that of Model C is the same as that of the stator. The cross-section shape of each pole of Models B and C is different from that of Model A, however, the sectional area of each pole of Models B and C is the same as that of Model A. The analyzed region is 1/8 of the whole region because of the symmetry and the periodicity. Fig. 3 shows the 3-D finite element meshes of Model A. In this analysis, the insulation between each core parts of Model A is considered by using the double node technique. Fig. 4 shows the setting positions of double nodes for the insulation of model A.

Fig. 5 shows the B-H curves used for the calculation of the nonlinear characteristics of the rotor and stator cores. Table II shows the analyzed conditions. In this paper, the effect of the material is analyzed when the revolution speed is assumed to 3,000, 5,000 and 10,000 rpm.

Table 1 Analysis Patterns

Model	A	B	C
Material of rotor and stator	SMC	silicon steel sheet	silicon steel sheet
Height of rotor	high	high	low

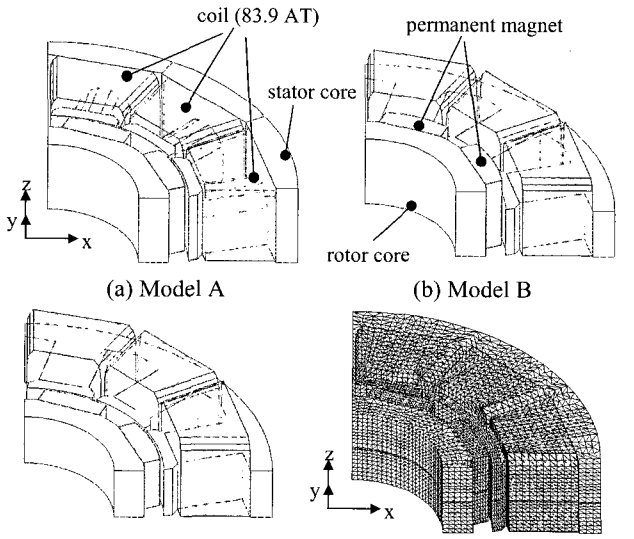

(a) Model A (b) Model B

(c) Model C

Fig. 2 Analyzed model.

Fig. 3 3-D finite element mesh (Model A).

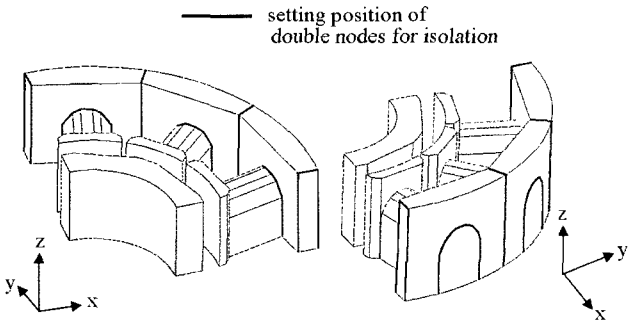

Fig. 4 Setting position of double nodes for insulation (Model A).

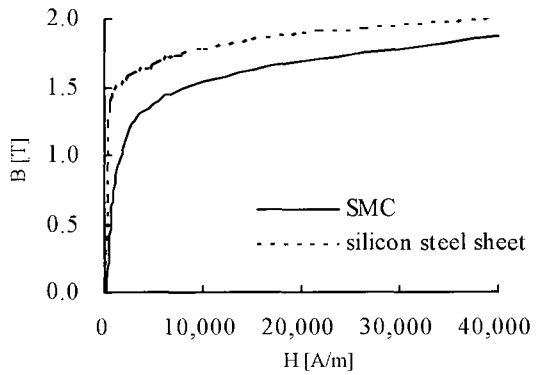

Fig. 5 B-H curves

Table 3 Analyzed Condition

Number of poles		8
Magnetization of magnet (T)		1.4
Revolution speed (rpm)		3,000, 5,000, 10,000
Exciting current (AT)		83.9
SMC	Conductivity (S/m)	1,000
	Density (kg/m^3)	7.35×10^3
Density of silicon steel sheet (kg/m^3)		7.85×10^3

3. Results and Discussion

Fig. 6 shows the distributions of flux density vectors when the revolution speed is 3,000 rpm. From these figures, it is found that the flux density vectors of the stator yoke of Model A are smaller than those of Models B and C. From o-a section as shown in Fig. 6(a)(ii), it is found that there are flux density at the part of the tip of the stator teeth is higher than in the stator. It is also found that the leakage flux of Model B is large, because the rotor is higher than the stator core.

Fig. 7 shows the distributions of eddy current density vectors of Model A when the revolution speed is 3,000 rpm.From these figures, it is found that the eddy currents in the rotor core is much smaller than in the stator, and the eddy current does not flow from one stator part to other ones due to the insulation.

Fig. 8 shows the contours of eddy current loss when the revolution speed is 3,000 rpm. From these figures, it is found that the eddy current loss of the rotor is much smaller than that of the stator. The eddy current loss of model A is much smaller than that of Model B and Model C. It is also found that there is much eddy current loss of Models B and C in the stator teeth surface. In Model B, the eddy current loss at the upper part in the stator surface is large, because the rotor is higher than the stator core.

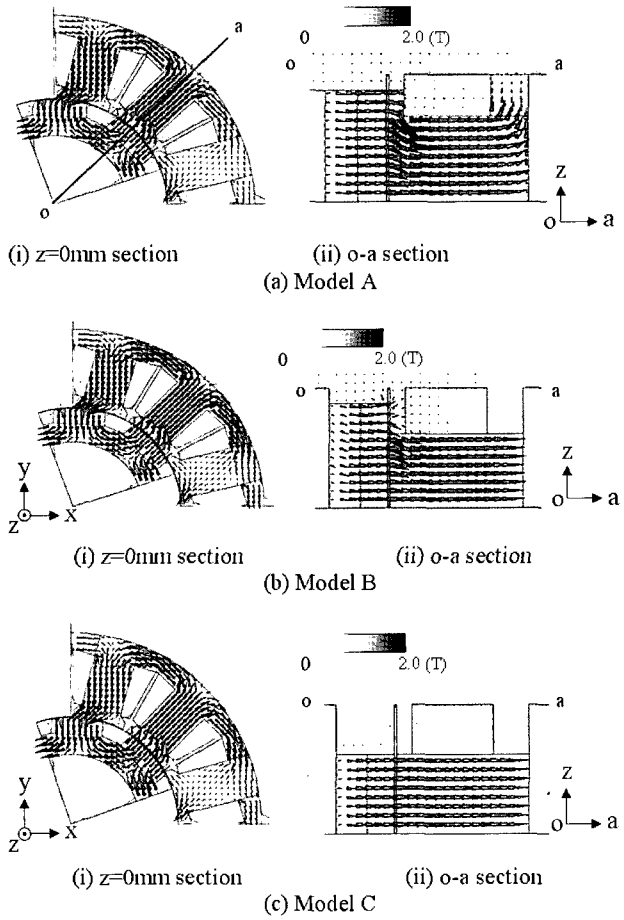

Fig. 6 Distributions of flux density vectors

Fig. 9 shows the contours of hysteresis loss when the revolution speed is 3,000 rpm. From these figures, it is found that the hysteresis loss of the Model A is larger than that of Models B and C. It is also found that there is much hysteresis loss in the stator teeth surface. In Model B, the hysteresis loss at the upper part in the teeth surface is large, because the rotor is higher than the stator core. The eddy current loss distributions are almost the same with the hysteresis loss. It means that the flux density at the upper part of the teeth is large.

Fig. 10 shows the torque characteristics. It is found that the torque ripple of Model A is larger than that of Models B and C.

It is also found that the average torque of Model A is almost the same as that of Model B, and Model C is the smallest of three models. In other words, the higher teeth and yoke are very effective to increase the average torque.

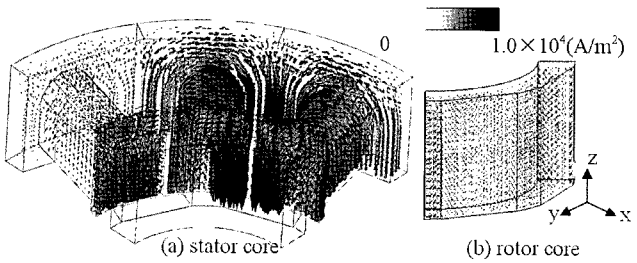

Fig. 7 Distributions of eddy current density vectors (Model A)

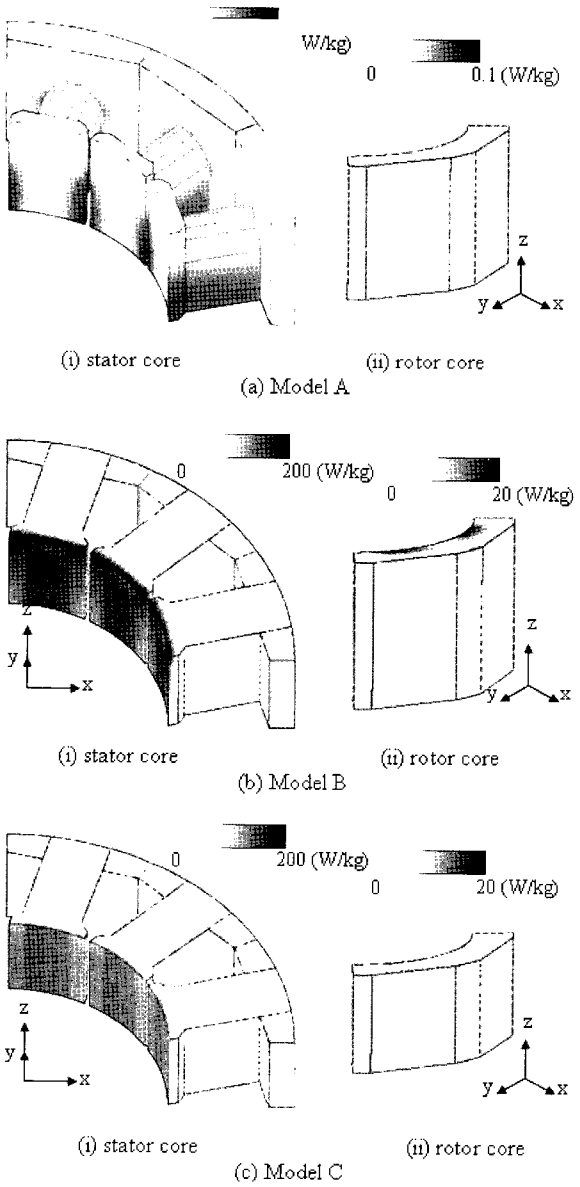

Fig. 8 Contours of eddy current loss

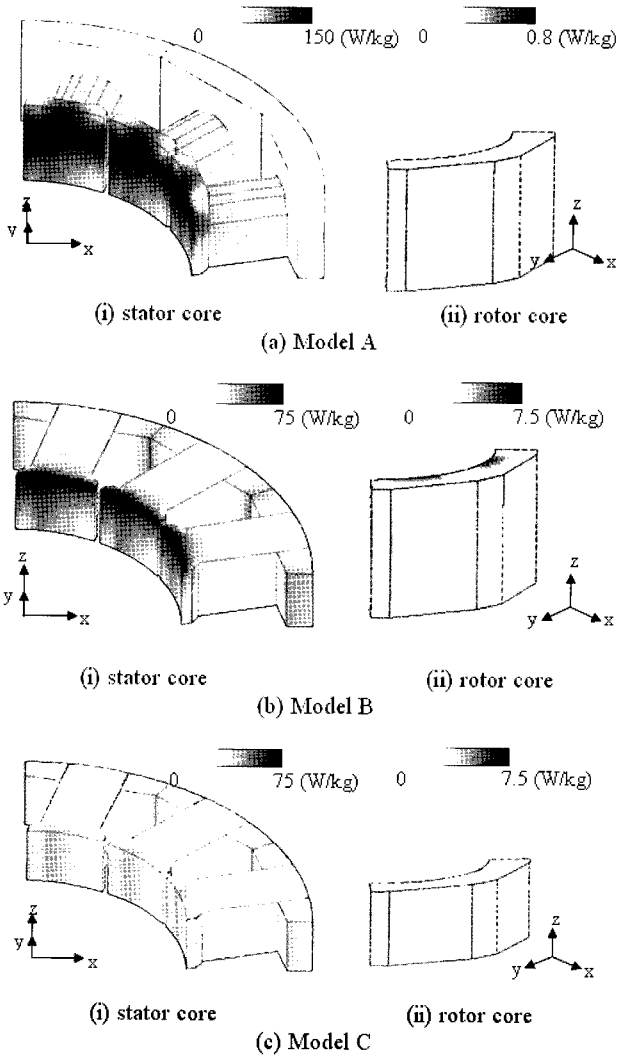

Fig. 9 Contours of hysteresis loss

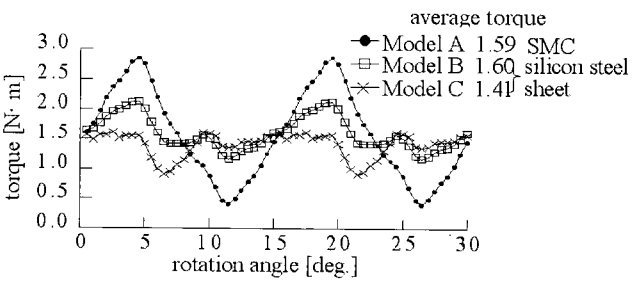

Fig. 10 Torque characteristics

Table 3 Discretization Data and CPU Time (Model A at 5,000 rpm).

Number of elements	427,392
Number of nodes	77,050
Number of edges	515,801
Number of unknown variables	505,575
Number of time steps	240
Total CPU time (hours)	127.6

Computer used: Pentium 4 (3.0GHz) PC

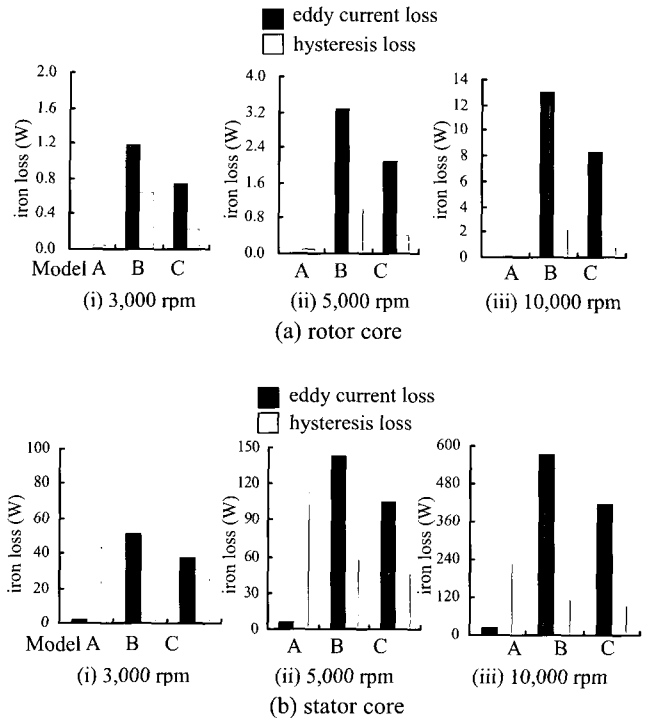

Fig. 11 Iron loss characteristics

Fig. 11 shows the iron loss characteristics. It is found that the eddy current loss of Model A is much smaller than those of Models B and C, although hysteresis loss of the stator core is large. The iron loss of the rotor core is much smaller than that of the stator core. It is also found that the hysteresis loss is proportional to frequency, and the eddy current loss is proportional to the frequency squared. In other words, the SMC is effective when the revolution speed is very high.

Table 2 shows the discretization data and CPU time.

4. Conclusion

In this paper, we calculated the surface permanent magnet motor made of the SMC using the 3-D finite element method. It is clarified that the eddy current loss is decreased using the SMC. It is found that it is effective when the revolution speed is very high, because eddy current loss is small though hysteresis loss is large. It is also clarified the usefulness of the SMC by comparing the silicon steel sheet.

References

[1] Patricia Jansson, "Processing Aspects of Soft Magnetic Composites", Euro PM 2000 Conference, 2000.

[2] S. Ito and Y. Kawase, *Computer Aided Engineering of Electric and Electronic Apparatus Using Finite Element Method*, Morikita Publishing Co., Tokyo, Japan, 2000.

[3] K. Yamazaki, "Efficiency Analysis of Induction Motor Considering Rotor and Stator Surface Loss Caused by Rotor Movement", *Proceedings of The 10th International Symposium on Applied Electromagnetics and Machines*, pp.107-108, 2001.

[4] Y. Kamiya and T. Onuki, "3-D Eddy Current Analysis by the Finite Element Method Using Double Nodes Technique", *IEEE Trans. Mag.*, Vol. 32, No. 3, pp. 741-744, 1996.

[5] A.G. Jack, B.C. Mecrow, P.G. Dickinson, D. Stephenson, J.S. Burdess, J.N. Fawcett and T. Evans, "Permanent Magnet Machines with Powdered Iron Cores and Pres-Pressed Windings", *Proceedings of IEEE 34th Annual Conference of Industry Applications Society*, Vol. 1, pp. 97-1031 1999.